Cell Reports

Report

Organized B cell sites in cartilaginous fishes reveal the evolutionary foundation of germinal centers

Graphical abstract

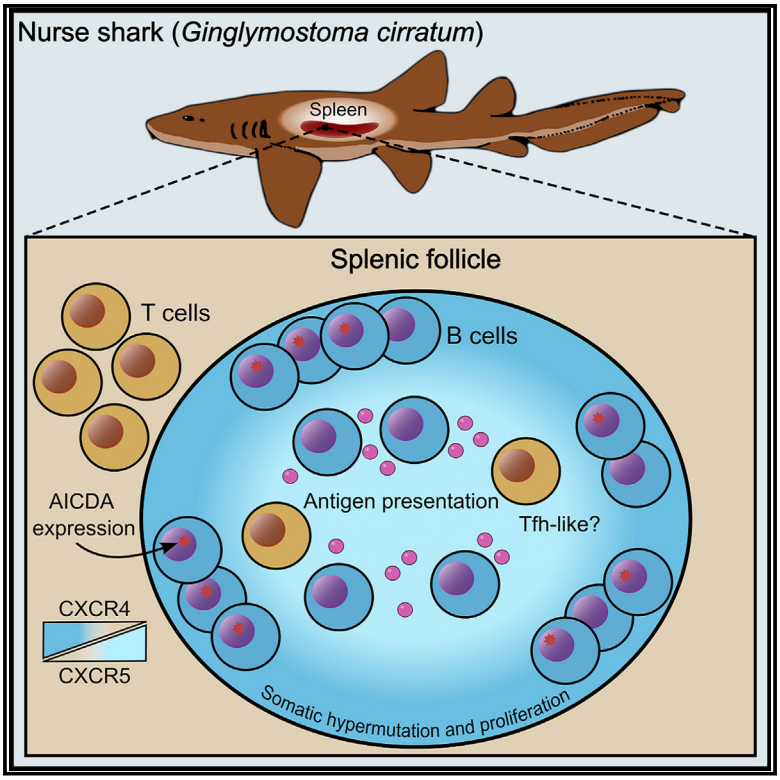

Authors

Hanover Matz, Richard S. Taylor, Anthony K. Redmond, ..., Neil C. Henderson, Daniel J. Macqueen, Helen Dooley

Correspondence

hdooley@som.umaryland.edu

In brief

Matz et al. studied the spleen of nurse sharks and found that functional hallmarks of mammalian germinal centers, including centrocyte- and centroblast-like B cells, a subset of T follicular helper-like cells, and cells that can present intact antigen, are present in the oldest jawed vertebrate lineage with adaptive immunity.

Highlights

- Shark splenic follicles share functional hallmarks of mammalian germinal centers
- Intact antigen accumulates in the center of splenic follicles post-immunization
- AID$^+$ CXCR4$^+$ centroblast-like B cells form a ring at the periphery of the follicles
- A population of shark T follicular helper-like cells were also identified

Matz et al., 2023, Cell Reports *42*, 112664
July 25, 2023
https://doi.org/10.1016/j.celrep.2023.112664

CellPress

Cell Reports

CellPress
OPEN ACCESS

Report

Organized B cell sites in cartilaginous fishes reveal the evolutionary foundation of germinal centers

Hanover Matz,[1] Richard S. Taylor,[2] Anthony K. Redmond,[3] Thomas M. Hill,[1] Rose Ruiz Daniels,[2] Mariana Beltran,[4] Neil C. Henderson,[4,5] Daniel J. Macqueen,[2] and Helen Dooley[1,6,*]

[1]Department of Microbiology and Immunology, University of Maryland School of Medicine, Institute of Marine and Environmental Technology, Baltimore, MD, USA

[2]The Roslin Institute and Royal (Dick) School of Veterinary Studies, University of Edinburgh, Edinburgh, UK

[3]Smurfit Institute of Genetics, Trinity College Dublin, Dublin, Ireland

[4]Centre for Inflammation Research, The Queen's Medical Research Institute, Edinburgh BioQuarter, University of Edinburgh, Edinburgh, UK

[5]MRC Human Genetics Unit, Institute of Genetics and Molecular Medicine, University of Edinburgh, Edinburgh, UK

[6]Lead contact

*Correspondence: hdooley@som.umaryland.edu

https://doi.org/10.1016/j.celrep.2023.112664

SUMMARY

The absence of germinal centers (GCs) in cartilaginous fishes lies at odds with data showing that nurse sharks can produce robust antigen-specific responses and affinity mature their B cell repertoires. To investigate this apparent incongruity, we performed RNA sequencing on single nuclei, allowing us to characterize the cell types present in the nurse shark spleen, and RNAscope to provide *in situ* cellular resolution of key marker gene expression following immunization with R-phycoerythrin (PE). We tracked PE to the splenic follicles where it co-localizes with CXCR5^{high} centrocyte-like B cells and a population of putative T follicular helper (Tfh) cells, surrounded by a peripheral ring of Ki67^{+} AID^{+} CXCR4^{+} centroblast-like B cells. Further, we reveal selection of mutations in B cell clones dissected from these follicles. We propose that the B cell sites identified here represent the evolutionary foundation of GCs, dating back to the jawed vertebrate ancestor.

INTRODUCTION

Cartilaginous fishes (Chondrichthyes; the sharks, rays, skates, and chimera) last shared a common ancestor with other jawed vertebrates over 450 million years ago[1] and are the oldest extant lineage to possess an adaptive immune system founded upon immunoglobulins (Igs), T cell receptors (TCRs), and major histocompatibility complex (MHC) molecules.[2] Based upon studies performed in the 1960s–1980s, it was widely held that the cartilaginous fish adaptive response was "primitive" compared with that of mammals.[3] This deficit was generally attributed to the absence of germinal centers (GCs), which are only histologically discernible in birds and mammals.[4]

GCs are specialized microanatomical structures that form within the B cell follicles of the mammalian spleen and lymph nodes following immunization or infection. Founded by antigen-specific B cells,[5] mammalian GCs are divided into two functionally distinct zones; CXCR4-expressing B cells in the dark zone (DZ), called centroblasts, undergo multiple rounds of rapid proliferation coupled with activation-induced cytidine deaminase (AICDA)-mediated somatic hypermutation (SHM) of their Ig genes. When centroblasts stop dividing, they migrate in a CXCR5-directed manner and enter the light zone (LZ) as centrocytes. The LZ contains a network of follicular dendritic cells (FDCs), which sequester unprocessed antigen on their surface. Centrocytes displaying higher affinity Igs can capture and present more antigen to the T follicular helper (Tfh) cells co-localized in the LZ and receive help to reenter the DZ for further rounds of proliferation/SHM. Concomitantly, some B cells exit the GC as antibody-secreting plasma cells and memory B cells.[6] Centrocytes that fail to bind antigen do not receive T cell help and undergo apoptotic cell death.

In vivo studies have since demonstrated that nurse sharks (*Ginglymostoma cirratum*) can produce robust, antigen-specific antibody responses and affinity mature their antibody repertoires, albeit on slower timescales than endotherms.[7,8] Durable immunological memory has also been confirmed in this species.[7,9] These findings raise the question of how sharks select antigen-specific B cell clones and affinity mature their Ig repertoires in the absence of GCs. To investigate this paradox, we performed RNA sequencing on single nuclei (snRNA-seq) from the nurse shark spleen, allowing us to characterize the cell types present, and RNAscope to provide *in situ* cellular resolution of key marker gene expression, following immunization with the fluorescent protein R-phycoerythrin (PE). Our results prove that the fundamental functional components found in mammalian GCs are also present in shark splenic follicles. We propose the B cell sites identified in nurse shark represent the evolutionary foundation of GCs.

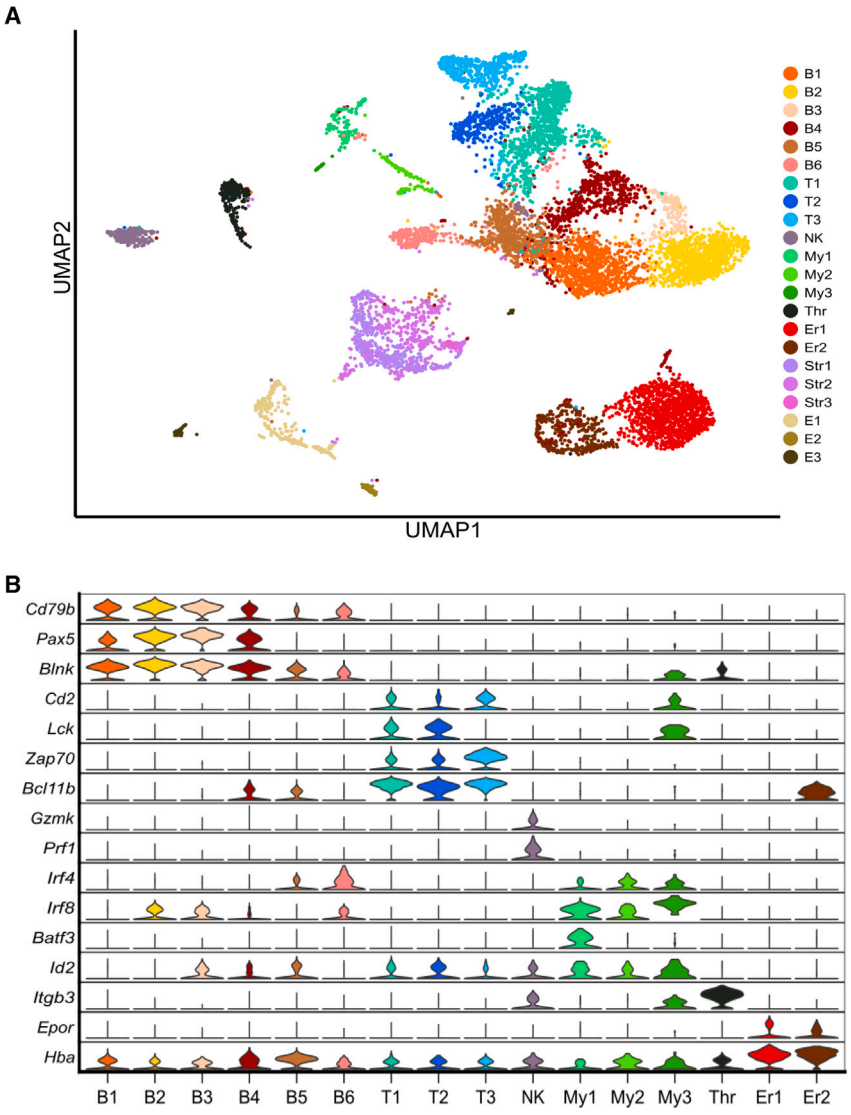

Figure 1. Single-cell transcriptome of the nurse shark spleen post-immunization

(A) Integrated UMAP plot of 22 transcriptionally distinct cell clusters gained using snRNA-seq from splenic tissue of two immunized nurse sharks.

(B) Violin plots showing the expression of key marker genes used to determine the identity of cell clusters.

RESULTS

Single-nucleus RNA sequencing reveals immune cell heterogeneity in shark spleen

While cartilaginous fishes hold a key phylogenetic position, being the most evolutionary distant group from mammals to also possess an Ig-based adaptive immune system,[2] surprisingly little is known of the immune cell types contributing to their immune responses. Thus, to determine the immune cell types present in the nurse shark spleen, we performed RNA sequencing on single nuclei (snRNA-seq) isolated from two animals, sacrificed at days 40 and 50 after subcutaneous immunization in the pectoral fin with PE (Figure 1A; Table S1). The sequence data were mapped against the whale shark (*Rhincodon typus*) genome,[10] the closest relative to the nurse shark with a high-quality annotated genome. Integrative analysis combining samples identified 22 unique cell clusters, representing 9,419 nuclei (Figure 1A; Table S1; Table S3). A list of marker genes for each cluster defined against the background of all other clusters is provided in Table S4; all loci are identified per their annotation in the whale shark genome.

Six distinct B cell clusters were identified (B1–B6), each showing significant transcript levels of *Cd79b* and *Blnk*, associated with B cell receptor (BCR) signaling, and *Pax5*, a master transcription factor for commitment to the B cell lineage (Figure 1B). T cells were present in 3 clusters (T1–T3) based on expression of the co-stimulatory receptor *Cd2*, genes associated with the TCR signaling complex including *Lck* and *Zap70*, and *Bcl11b*, encoding a transcription factor associated with T cell development (Figure 1B). The T cell clusters also showed high transcript levels of T cell-associated transcription factors *Runx3*, *Gata3*, and *Nfatc2* (Table S4). Several clusters (My1–My3) were attributed to the myeloid lineage based upon expression of transcription factors associated with macrophage-/DC-like fates, including *Irf4*, *Irf8*, *Batf3*, and *Id2* (Figure 1B). A single natural killer (NK) cell cluster was identified based upon the expression of perforin 1 (*Prf1*) and granzyme-K-like (*Gzmk*) loci but low/no expression of TCR-associated genes. Both erythrocytes and thrombocytes are nucleated in cartilaginous fishes[11]; accordingly, we identified two erythrocyte clusters (Er1 and Er2), based upon erythropoietin receptor (*Epor*) and high levels of hemoglobin alpha (*Hba*) transcript, and a single thrombocyte (Thr) cluster based on *Itgb3* transcript. The remaining non-immune cell clusters are likely endothelial/epithelial-like cells of the vasculature (E1–E3; expressing *Vegfr-1*, *Abi3bp*, and *Stab1*) and stroma (Str1-Str3; expressing *Npnt*, *Wt1*, and *St5*).

Shark B cell subpopulations exhibit centrocyte- and centroblast-like transcript profiles and are spatially segregated in splenic follicles

Given the presence of multiple B cell clusters in our uniform manifold approximation and projection (UMAP), we examined the list of genes differentially expressed in each B cell cluster, attempting to classify them in finer detail. Cluster B2 exhibited markedly higher transcript levels of *Flt3*, a cytokine receptor up-regulated on activated B cells,[12,13] compared with cluster B1

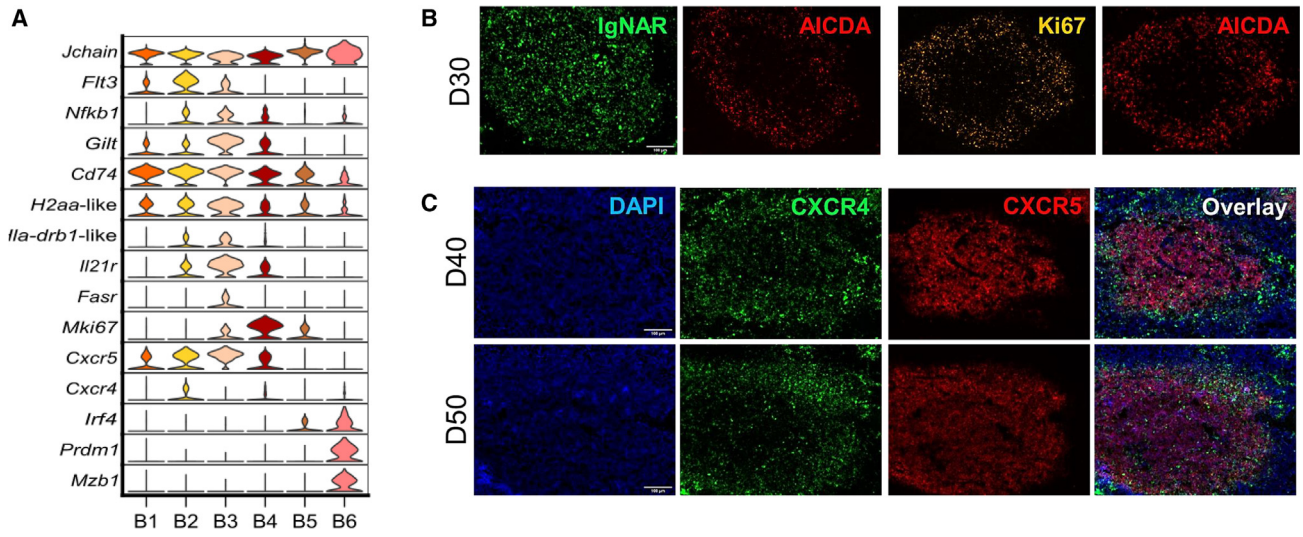

Figure 2. Characterization of B cell clusters identified in nurse shark spleen and expression of AID in the splenic follicles

(A) Violin plots showing the expression of key marker genes used to characterize B cell clusters.

(B) RNA FISH microscopy images showing transcript patterns of *Ignar* (green), *Aicda* (red), and *Mki67* (yellow) in B cell follicles of nurse shark spleen at day 30 post-immunization.

(C) RNA FISH microscopy images showing transcript patterns of *Cxcr4* (green) and *Cxcr5* (red) in nurse shark spleen at days 40 and 50 post-immunization. Cell nuclei are stained with DAPI (blue). Scale bar, 100 μm in all images.

(Figure 2A). Cluster B2 also expressed higher *Nfkb1* than cluster B1, indicative of nuclear factor κB (NF-κB) signaling, which occurs downstream of BCR-antigen engagement,[14] along with multiple members of the MAP kinase cascade (Table S4). Thus, cluster B1 likely represents naive splenic B cells, while cluster B2 represents antigen-experienced, activated B cells.

Cluster B3 cells were enriched for transcripts associated with antigen presentation via the MHC class II pathway. These included *Gilt*, a lysosomal thiol reductase that facilitates antigen processing; *Cd74*, the invariant chain associated with MHC II-peptide complex formation; and loci annotated as mouse *H2aa*-like and human *Hla-drb1*-like MHC class II chains (Figure 2A). Further, *Il21r* and *Fasr* were transcribed at a markedly higher level in cluster B3 compared with the other B cell clusters (Figure 2A). Together, these data suggest that B3 cells are centrocyte-like, being able to present antigen to helper T cells for selection via the MHC class II pathway and, in turn, receive survival signals in the form of co-stimulation and interleukin-21 (IL-21) signaling via the IL-21 receptor (IL-21R)[15] or be eliminated from the selective process through Fas-mediated apoptosis.[16] In contrast, cluster B4 cells exhibited much higher transcript levels of the proliferation marker *Mki67* than other B cell clusters (Figure 2A), along with many other genes associated with proliferation and mitosis (Table S4). Cluster B4 thus appears to correspond to actively proliferating centroblast-like B cells.

Given that AICDA is a definitive marker of hypermutating centroblasts,[17] and shark Ig transcripts show very high levels of SHM,[18] it was surprising that cluster B4 (or any other B cell cluster) showed no expression of *Aicda*. However, inspection of the whale shark genome annotation used for snRNA-seq revealed that it lacked the *Aicda* gene, and despite efforts to add the nurse shark gene to our analysis manually (see STAR Methods), we failed to identify significant expression in any nurse shark B cells within the limits of snRNA-seq. Therefore, to ascertain if any B cells in the nurse shark spleen express AICDA, we designed RNAscope probes for nurse shark *Aicda* and *Ignar*, a heavy chain-only Ig isotype found in sharks.[19] AICDA transcript was detected within the splenic B cell follicles of every animal sampled, regardless of time point (Figure S2A), with the cells transcribing *Aicda* forming a ring at the periphery of the follicle and overlapping nurse shark *Mki67* transcription (Figures 2B and S2B).

In mammalian GCs, expression of the chemokine receptor CXCR4 directs centroblasts to the DZ, while CXCR5 retains centrocytes in the LZ. Correspondingly, in our dataset, cluster B3 exhibited higher transcript levels of *Cxcr5* than cluster B4, while cluster B4 displayed low levels of *Cxcr4* transcript (Figure 2A). Probing spleen sections for *Cxcr4* and *Cxcr5* transcripts[20] revealed that nurse shark B cell follicles possess a central $CXCR5^+$ zone transitioning to a peripheral $CXCR4^+$ zone (Figures 2C and S2C), the latter overlapping our previously noted zone of AICDA/Ki67 transcription (Figure S2D). Together, these results confirm that the nuclei of cluster B4 are highly proliferative, AICDA-expressing centroblast-like B cells that likely segregate to the periphery of the follicle in a CXCR4-directed fashion.

Finally, we inferred B cell clusters B5 and B6 to be plasmablasts and plasma cells, respectively. Both clusters showed dramatically reduced *Pax5* transcript levels (Figure 1B) with up-regulation of *Irf4*, a master transcription factor critical for the development and maintenance of plasma cells (Figure 2A). Cluster B6 also exhibited high *Prdm1* (the gene encoding Blimp1) and *Mzb1* (a co-chaperone) transcript levels, indicating high-level secretory Ig production (Figure 2A).

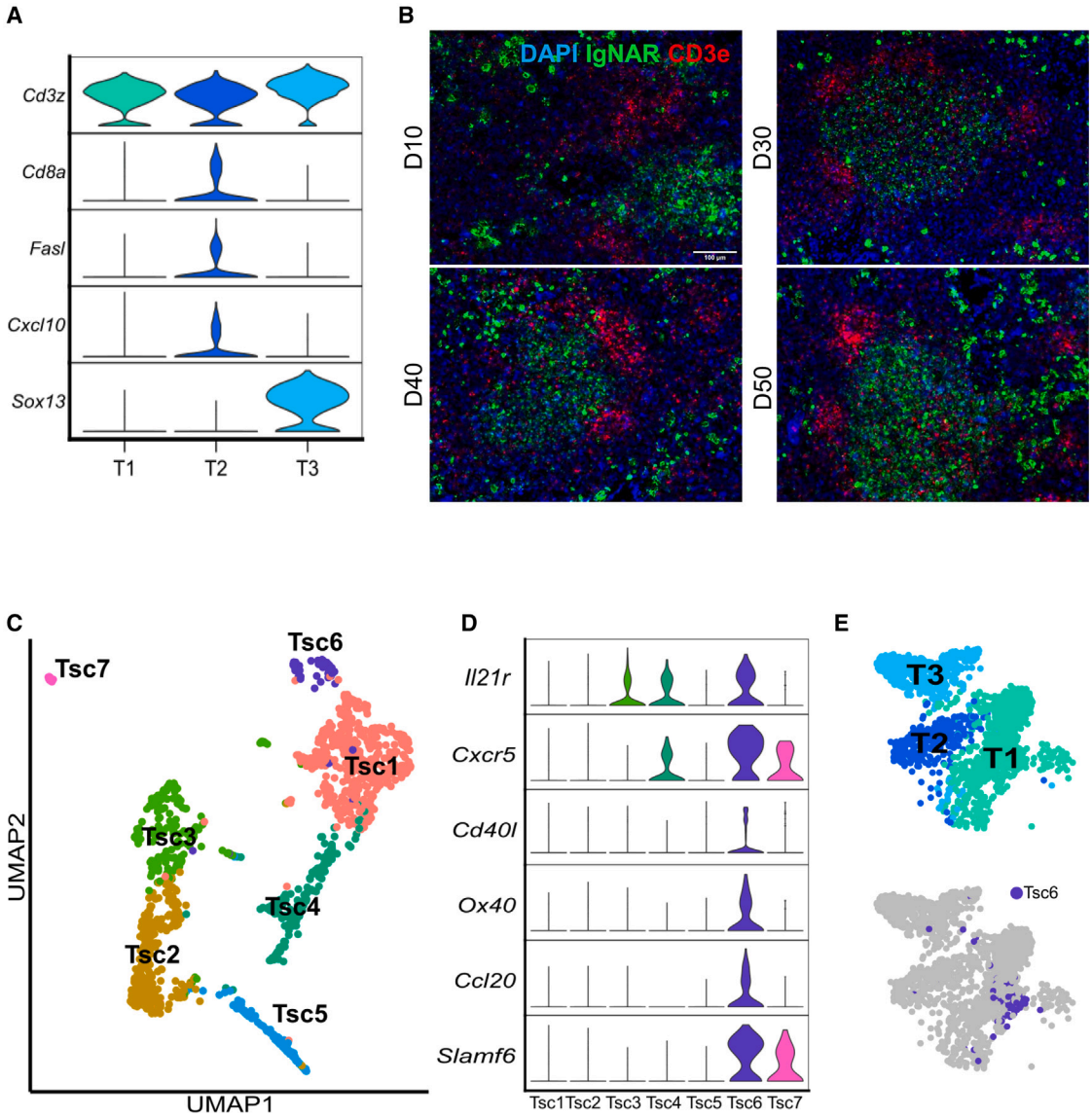

Figure 3. Characterization of T cell clusters and a population of T follicular helper (Tfh)-like cells in the nurse shark spleen

(A) Violin plots showing the expression of key marker genes used to characterize T cell clusters.

(B) RNA FISH microscopy images showing transcript patterns of *Ignar* (green) and *Cd3e* (red) in nurse shark spleen at days 10–50 post-immunization. Cell nuclei are stained with DAPI (blue). Scale bar,100 μm.

(C) UMAP performed after subclustering of T cells extracted from the global dataset.

(D) Violin plots showing the expression of marker genes corresponding to Tfh cell function in mammals in T cell subclusters.

(E) UMAP plot of the original T cell clusters (Figure 1A), demonstrating that Tsc6 is largely found within T cell cluster T1.

Sharks possess a T cell subset with phenotypic resemblance to mammalian Tfh cells

As detailed above, three UMAP clusters were identified as T cells (T1–T3), all exhibiting high transcript levels of the TCR signaling complex molecule *Cd3z* (Figure 3A). The specific expression of *Cd8a* in cluster T2 is consistent with a CD8 killer T cell population. While T2 lacks expression of genes encoding perforin 1 or granzyme-K-like, it does show specific expression of *Fasl*, associated with Fas-mediated T cell cytotoxicity,[21,22] as well as the proinflammatory cytokine *Cxcl10*,[23] suggesting CD8 killer T cell-like functionality. We also identified cluster T3 as a likely γδ T cell population based on expression of *Sox13*, a master transcription factor that regulates γδ T cell and γδ-like cell fate in both jawed and jawless vertebrates.[24,25] CD4 has not been found in any cartilaginous fish species examined to date,[26] but there is evidence for CD4 helper T cell subsets in cartilaginous fishes.[27] Based upon the presence of *Cd3z* and the absence of *Cd8a*/*Sox13*, the cells in cluster T1 are most likely the shark equivalent of mammalian CD4 helper cells.

To explore the spatial distribution of T cells within the shark spleen, we designed RNAscope probes for nurse shark *Cd3*e, a TCR signaling component retained as a single copy gene in nurse shark.[28] Probing for *Cd3e* transcript revealed (1) aggregates of T cells localized in the extrafollicular space, which, particularly at later time points (days 30–50) post-immunization, associate more closely with the borders of B cell follicles, and (2) individual CD3e$^+$ cells dispersed throughout the B cell follicles (Figure 3B), a distribution reminiscent of mammalian Tfh cells in GCs.

Based upon the presence of many T cell subset-defining molecules in cartilaginous fish sequence datasets, it is predicted that sharks can generate a mammalian-like repertoire of T helper subsets, including a Tfh-like subset.[27] We therefore performed a subcluster analysis on the original T1–T3 clusters to explore additional cellular heterogeneity and to attempt to identify a Tfh-like subset (Figure 3C). Seven distinct T cell subclusters (Tsc1–Tsc7) were identified, with Tsc6 (comprising 90 nuclei) expressing numerous markers indicative of a Tfh-like phenotype (Figures 3C and 3D). These included *Cxcr5* and *Cd40l*, suggesting that Tsc6 cells localize to B cell follicles and can provide co-stimulatory signals. Tsc6 also specifically expressed *Ox40* and *Il21r*, both markers of mammalian Tfh cells.[29,30] Finally, Tsc6 specifically expressed the chemokine ligand *Ccl20* and the adhesion molecule *Slamf6*, both of which promote stable Tfh-B cell interactions in mammals.[31,32] The nuclei composing this subcluster were primarily derived from the T1 cluster, our hypothesized shark CD4-like cells (Figure 3E). Collectively, the snRNA-seq and fluorescence *in situ* hybridization (FISH) data indicate that Tsc6 is a shark Tfh-like subset capable of providing co-stimulatory signals to B cells to facilitate clonal selection. Further, our data suggest the presence of other CD4$^+$-equivalent T cell subsets among the subclusters, but a more comprehensive annotation of T cell subset-discriminating cytokines in shark genomes, a non-trivial task,[26,27,33] is required to make definitive identifications.

The shark spleen contains cells capable of presenting intact antigen to B cells

While clonal selection is facilitated by survival signals from Tfh cells, it also requires the presentation of antigen by specialized antigen-presenting cells (APCs) allowing B cells to test their BCR for antigen specificity.[6] In mammals, these APCs are FDCs, which, unlike conventional DCs (cDCs) derived from bone marrow hematopoietic stem cells, are of stromal origin.[34] FDCs capture and retain antigen in immune complexes with minimal degradation to preserve non-linear epitopes for BCR recognition.[35,36] Thus far, true FDCs have only been found in mammals and birds; however, it is increasingly apparent that some mammalian cDCs can present intact antigen.[37] Here, we sought to determine if any of the myeloid cells present in the nurse shark spleen might present intact antigen to facilitate B cell clonal selection.

Our snRNA-seq data revealed that My1–My3 expressed genes associated with MHC class II antigen presentation, including *H2aa*-like and *Hla-drb1*-like loci, *Gilt*, and *Cd74* (Figure 4A), indicating that these cells could function as professional APCs. Further, APC-associated markers expressed in myeloid clusters include *Cd83*, generally expressed on activated DCs,[38] the genes encoding integrin alpha M and integrin alpha X (*Cd11b* and *Cd11c*, respectively); *Icam3*, a cell adhesion molecule; and *Cd9*, a tetraspanin expressed in APCs.[39,40] Expression of the complement Ig receptor gene *Vsig4* was found across My1–My3, but no other complement receptors or IgFc receptors were present among the cluster-defining transcripts (Figure 4A). This was not altogether surprising given that these receptor families evolve quickly and so their identification in non-mammalian species is challenging. However, the absence of such markers makes it difficult to predict if any of the myeloid cell clusters within our snRNA dataset can capture immune complexes and present intact antigen.

Requiring a different approach, we took advantage of the fact that PE, the antigen used for immunization, is fluorescent when intact. Spleen sections taken from the sharks at days 10, 30, 40, and 50 post-immunization were stained with monoclonal antibodies raised against nurse shark IgL, effectively labeling all IgM$^+$ B cells, or IgNAR, which lacks IgL (Figure S3A). While a PE signal was not found in the B cell follicles at day 10, large particles of PE are observed predominantly within extrafollicular space at day 30 (Figure 4B). By day 40, a reticular pattern of the PE signal was observed in the center of approximately half of the splenic B cell follicles (Figures 4B, S3B, and S3C). Unfortunately, we did not observe this pattern of antigen presentation in the day 50 animal, although antigen was present in the extrafollicular space (Figure 4B). However, slight variation in the timing of the response between individuals is unsurprising given that these are unrelated, outbred animals. Regardless, our data show that nurse sharks are capable of trafficking antigen from the periphery to the splenic B cell follicles, where it is presented in a non-degraded form that preserves epitopes for BCR recognition.

VNAR clones isolated from nurse shark splenic follicles show selection of mutations in B cell clones

If shark splenic follicles support the selection of antigen-specific B cell clones in a manner akin to mammalian GCs,[6] we would predict a similar bias in the mutational profile of shark Ig variable (V) regions.[41] To test this hypothesis, we used laser microdissection (LMD) to isolate IgNAR$^+$ follicles from spleen sections of the animal sacrificed at day 40 post-immunization and which showed follicular PE presentation (Figure 4B). Using PCR primers targeting the framework regions, we amplified and sequenced IgNAR V regions (VNARs) from these follicles using Illumina sequencing, recovering ~230,000 functional V segment open reading frames (ORFs), encoding ~1,500 unique VNARs.

Shark IgNAR genes are arranged in clusters, each containing a single V segment, three diversity (D) segments, and a joining (J) segment. The V segment lacks CDR2 but, in addition to CDR1, encodes two additional hypervariable (HV) loops, designated HV2 and HV4, which can also participate in antigen binding.[42] Using our VNAR dataset, we examined amino acid variability compared with germline across the length of the V segment. By the Wu-Kabat variability coefficient,[43] variability was significantly greater in the CDR/HVs than the framework regions (FRs) (Figure 4C). This was more apparent when only the top 100 most abundant VNARs (representing ~185,000

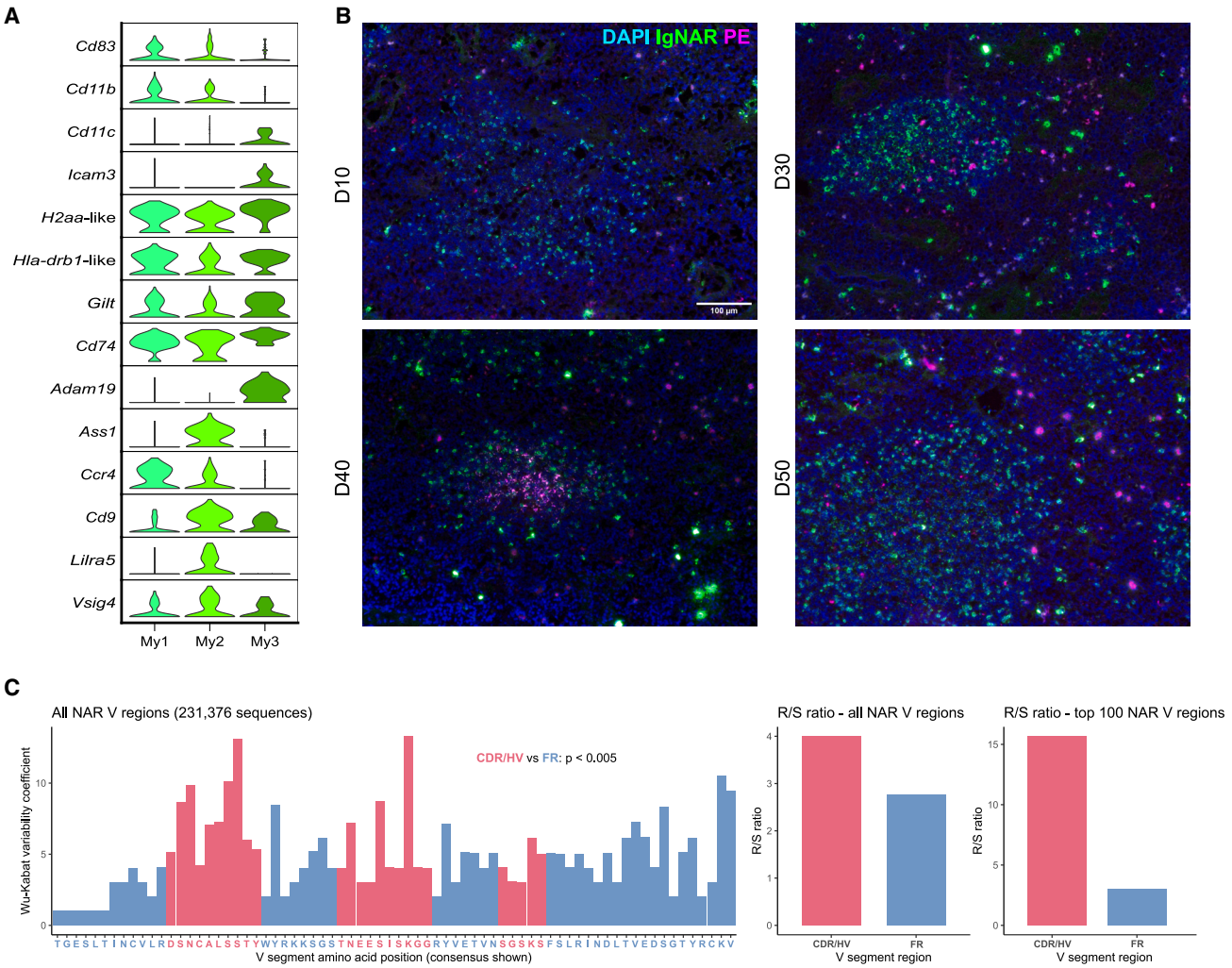

Figure 4. Presentation of non-degraded antigen in nurse shark spleen permits B cell selection

(A) Violin plots showing the expression of key marker genes used to characterize myeloid cell clusters.

(B) Fluorescence microscopy images showing phycoerythrin (PE; magenta) moving into IgNAR$^+$ (green) B cell follicles and accumulating in the follicular center around day 40 post-immunization. Cell nuclei are stained with DAPI (blue). Scale bar, 100 μm.

(C) Wu-Kabat amino acid variability across all distinct NAR V region sequences isolated by LMD, showing comparison of the FRs compared with the CDR/HVs (left). p values shown are for Wilcoxon rank-sum test of all CDR/HV sites vs. all FR sites. R/S ratios of the CDR/HVs and FRs of all distinct NAR V region sequences (middle) and the top 100 most abundant distinct NAR V region sequences (right).

sequences), clones that have probably undergone selection and received help to proliferate, were analyzed (Figure S3D). The ratio of replacement-to-silent mutations (R/S) is also used as a measure of antigen-driven positive selection. We observed a higher R/S ratio in the CDR/HVs than the FRs of our VNAR dataset (Figure 4C). Our results confirm a bias toward replacement mutations in the VNAR CDR/HV regions in clones isolated from shark B cell follicles.

DISCUSSION

Prior to this study, the reported absence of GCs,[44,45] or potentially analogous structures,[46] in cartilaginous fishes lay at odds with accumulating data showing that sharks can produce robust antigen-specific responses following immunization, affinity mature their B cell repertoires, and maintain immunological memory for many years.[7–9] Here, we demonstrate that cartilaginous fishes and, by inference, the common jawed vertebrate ancestor possess(ed) many of the fundamental components for B cell selection as are found in the GCs of endothermic vertebrates, specifically (1) populations of AID-expressing, CXCR4$^+$ centroblast-like, and CXCR5-high centrocyte-like B cells; (2) cells with functional similarity to mammalian Tfh cells that express many genes with roles in co-stimulation and B cell clonal selection; (3) professional APCs possessing some mechanism for presenting non-degraded antigen, thus permitting the selection of BCRs against multiple epitopes; and (4) evidence of CDR-biased mutation following AID-mediated SHM of Ig genes. Combined, our data

suggest that shark B cell clones compete for antigen binding and co-stimulatory signals from Tfh-like cells in the center of the follicle before migrating in a CXCR4-directed fashion to the periphery of the follicle to proliferate and mutate their receptors. Whether shark B cells move between these two stages in iterative rounds of Darwinian selection, akin to the LZ/DZ cycling of mammalian GC reactions[6] before exiting as fully differentiated plasma or memory cells, will be difficult to determine. However, shark Ig transcripts show exceptionally high rates of SHM,[18,47] and families of antigen-specific IgNAR clones have been found that share many mutations in common but are uniquely mutated at multiple other sites.[8] This strongly suggests that shark B cells undergo limited rounds of selection with high mutational loads per round, a strategy that would rapidly diversify any antigen-specific B cell clones present.

We propose that the B cell sites identified herein represent the evolutionary foundation of GCs. However, unlike mammalian GCs, which are founded by antigen-specific B cells and form as a distinct structure within the follicle, B cell selection in sharks utilizes the whole follicle. Our RNAscope data suggest that BCR mutation and selection proceed in a continuous manner as antigens move from the periphery into the shark spleen, much as occurs in the chronic GCs of mammalian gut Peyer's patches.[48,49] This implies that the antigenic profile of each follicle, and the B cells selected therein, shifts over time as captured antigen is replaced/displaced by newer antigens, as recently shown to occur in mouse lymph nodes.[50] We hypothesize that wide distribution of antigen creates a more permissive selection environment for antigen-specific B cells than is found in mammalian GCs, thus facilitating the retention of lower affinity clones and supporting the production of an extensive and diverse memory B cell pool.[51] This perhaps explains the reportedly low increases in antibody affinity over the course of a primary response in cartilaginous fishes and other ectothermic vertebrates.[8]

Together, our data offer support for the suggestion[52] that the main advantage of SHM/selection in cartilaginous fishes, and, by inference, the jawed vertebrate ancestor, is/was the generation of a diverse memory B cell repertoire. If true, then what selective advantage did the evolution of GCs confer upon birds and mammals? We predict that the distinct microanatomical structure of the GC better focuses the selection process, increasing competition for antigen and T cell help, thereby facilitating faster, more efficient, selection of higher affinity antigen-specific B cells. Indeed, the GCs of birds are organized much like the nurse shark B cell follicles described herein, with a central "LZ-like" region and peripheral "DZ-like" ring containing proliferating B cells,[53] but on a smaller scale. Certainly, antigen-specific antibody titers peak much earlier in mammals (days to weeks) than sharks (months),[7] likely providing an advantage following the switch to endothermy and faster replication of potential pathogens. Importantly, our work shows that highly organized B cell sites in splenic follicles existed at least 200 million years before the evolution of GCs.

Limitations of the study

We are permitted by special license to take only a very small number of sharks from the wild. These are outbred, unrelated animals with unknown exposure histories, and, consequently, the timing and magnitude of their responses vary considerably. Thus, while the main conclusions of our study remain firm, the precise timing of events (e.g., the display of antigen within the follicles) naturally differs between individuals. Thus, while we hypothesize chronic B cell mutation and selection against a constant flow of unprocessed antigens, this will be difficult to test experimentally given the limited availability of sharks, the individual variation detailed above, and the necessity for (terminal) spleen tissue samples. Finally, while our VNAR mutation analyses support the antigen-driven selection of B cell clones in shark splenic follicles, the binding specificity of these clones was not established. We intended to build phage-displayed VNAR libraries, pan these for PE-specific clones, and explore the mutation profiles and affinities of these clones. Unfortunately, due to the very low yield of RNA from the laser-dissected splenic follicles, this was not possible. We will keep this experiment in mind when designing future studies.

STAR★METHODS

Detailed methods are provided in the online version of this paper and include the following:

- KEY RESOURCES TABLE
- RESOURCE AVAILABILITY
  - Lead contact
  - Materials availability
  - Data and code availability
- EXPERIMENTAL MODEL AND STUDY PARTICIPANT DETAILS
  - Animals
- METHOD DETAILS
  - Shark immunizations and sample collection
  - Immunofluorescence microscopy
  - Fluorescence *in situ* hybridization (FISH)
  - snRNA-seq data generation and analysis
  - Rapid immunofluorescence staining and laser microdissection (LMD)
  - LMD IgNAR variable region repertoire data generation and analysis
- QUANTIFICATION AND STATISTICAL ANALYSIS

SUPPLEMENTAL INFORMATION

Supplemental information can be found online at https://doi.org/10.1016/j.celrep.2023.112664.

ACKNOWLEDGMENTS

Our thanks to Masahiro Iwamoto and his team (University of Maryland, Baltimore) for granting us access to their Leica LMD7 microscope, providing training, and sharing their extensive expertise with us. Our thanks also to Martin Flajnik (University of Maryland, Baltimore) for providing the GA10, NARV, and LK14 antibody supernatants used in our immunofluorescence microscopy experiments. We thank Clara Pereira (Trinity College Dublin) for advice on using MiXCR. This work was funded by National Institutes of Health Institutional Training Grant T32AI095190 (H.M.), National Institutes of Health Predoctoral Fellowship F31AI147532 (H.M.), Irish Research Council Postdoctoral Fellowship GOIPD/2021/466 (A.K.R.), Wellcome Trust Senior Research Fellowship 219542/Z/19/Z (N.C.H.), BBSRC institutional strategic program funding

BBS/E/D/20002174 awarded to The Roslin Institute, and the IMET Innovations in Science Program, sponsored by the G. Unger Vetlesen Foundation (H.D.).

AUTHOR CONTRIBUTIONS

Conceptualization, H.M. and H.D.; methodology, H.M., R.S.T., R.R.D., A.K.R., M.B., and H.D.; investigation, H.M., R.S.T., A.K.R., T.M.H., R.R.D., M.B., and H.D.; formal analysis, H.M., R.S.T., A.K.R., D.J.M., and H.D.; visualization, H.M., R.S.T., A.K.R., and T.M.H.; funding acquisition, H.M., D.J.M., N.C.H., and H.D.; resources, N.C.H., D.J.M., and H.D.; supervision, N.C.H., D.J.M., and H.D.; writing – original draft, H.M. and H.D.; writing – review & editing, all authors.

DECLARATION OF INTERESTS

The authors declare no competing interests.

Received: April 19, 2022
Revised: February 28, 2023
Accepted: June 4, 2023
Published: June 20, 2023

REFERENCES

1. Irisarri, I., Baurain, D., Brinkmann, H., Delsuc, F., Sire, J.-Y., Kupfer, A., Petersen, J., Jarek, M., Meyer, A., Vences, M., et al. (2017). Phylotranscriptomic consolidation of the jawed vertebrate timetree. Nat. Ecol. Evol. *1*, 1370–1378. https://doi.org/10.1038/s41559-017-0240-5.
2. Flajnik, M.F. (2018). A cold-blooded view of adaptive immunity. Nat. Rev. Immunol. *18*, 438–453. https://doi.org/10.1038/s41577-018-0003-9.
3. Dooley, H., and Flajnik, M.F. (2006). Antibody repertoire development in cartilaginous fish. Dev. Comp. Immunol. *30*, 43–56. https://doi.org/10.1016/j.dci.2005.06.022.
4. Neely, H.R., and Flajnik, M.F. (2016). Emergence and evolution of secondary lymphoid organs. Annu. Rev. Cell Dev. Biol. *32*, 693–711. https://doi.org/10.1146/annurev-cellbio-111315-125306.
5. Pereira, J.P., Kelly, L.M., Xu, Y., and Cyster, J.G. (2009). EBI2 mediates B cell segregation between the outer and centre follicle. Nature *460*, 1122–1126. https://doi.org/10.1038/nature08226.
6. Mesin, L., Ersching, J., and Victora, G.D. (2016). Germinal center B cell dynamics. Immunity *45*, 471–482. https://doi.org/10.1016/j.immuni.2016.09.001.
7. Dooley, H., and Flajnik, M.F. (2005). Shark immunity bites back: affinity maturation and memory response in the nurse shark, Ginglymostoma cirratum. Eur. J. Immunol. *35*, 936–945. https://doi.org/10.1002/eji.200425760.
8. Dooley, H., Stanfield, R.L., Brady, R.A., and Flajnik, M.F. (2006). First molecular and biochemical analysis of in vivo affinity maturation in an ectothermic vertebrate. Proc. Natl. Acad. Sci. USA *103*, 1846–1851. https://doi.org/10.1073/pnas.0508341103.
9. Eve, O., Matz, H., and Dooley, H. (2020). Proof of long-term immunological memory in cartilaginous fishes. Dev. Comp. Immunol. *108*, 103674. https://doi.org/10.1016/j.dci.2020.103674.
10. Tan, M., Redmond, A.K., Dooley, H., Nozu, R., Sato, K., Kuraku, S., Koren, S., Phillippy, A.M., Dove, A.D., and Read, T. (2021). The whale shark genome reveals patterns of vertebrate gene family evolution. Elife *10*, e65394. https://doi.org/10.7554/eLife.65394.
11. Arnold, J.E. (2005). Hematology of the sandbar shark, Carcharhinus plumbeus: standardization of complete blood count techniques for elasmobranchs. Vet. Clin. Pathol. *34*, 115–123. https://doi.org/10.1111/j.1939-165x.2005.tb00023.x.
12. Svensson, M.N.D., Andersson, K.M.E., Wasén, C., Erlandsson, M.C., Nurkkala-Karlsson, M., Jonsson, I.-M., Brisslert, M., Bemark, M., and Bokarewa, M.I. (2015). Murine germinal center B cells require functional Fms-like tyrosine kinase 3 signaling for IgG1 class-switch recombination. Proc. Natl. Acad. Sci. USA *112*, E6644–E6653. https://doi.org/10.1073/pnas.1514191112.
13. Kallies, A., Hasbold, J., Fairfax, K., Pridans, C., Emslie, D., McKenzie, B.S., Lew, A.M., Corcoran, L.M., Hodgkin, P.D., Tarlinton, D.M., et al. (2007). Initiation of plasma-cell differentiation is independent of the transcription factor Blimp-1. Immunity *26*, 555–566. https://doi.org/10.1016/j.immuni.2007.04.007.
14. Pontoriero, M., Fiume, G., Vecchio, E., de Laurentiis, A., Albano, F., Iaccino, E., Mimmi, S., Pisano, A., Agosti, V., Giovannone, E., et al. (2019). Activation of NF-κB in B cell receptor signaling through Bruton's tyrosine kinase-dependent phosphorylation of IκB-α. J. Mol. Med. *97*, 675–690. https://doi.org/10.1007/s00109-019-01777-x.
15. Gonzalez, D.G., Cote, C.M., Patel, J.R., Smith, C.B., Zhang, Y., Nickerson, K.M., Zhang, T., Kerfoot, S.M., and Haberman, A.M. (2018). Nonredundant roles of IL-21 and IL-4 in the phased initiation of germinal center B cells and subsequent self-renewal transitions. J. Immunol. *201*, 3569–3579. https://doi.org/10.4049/jimmunol.1500497.
16. Hao, Z., Duncan, G.S., Seagal, J., Su, Y.-W., Hong, C., Haight, J., Chen, N.-J., Elia, A., Wakeham, A., Li, W.Y., et al. (2008). Fas receptor expression in germinal-center B cells is essential for T and B lymphocyte homeostasis. Immunity *29*, 615–627. https://doi.org/10.1016/j.immuni.2008.07.016.
17. Muramatsu, M., Kinoshita, K., Fagarasan, S., Yamada, S., Shinkai, Y., and Honjo, T. (2000). Class switch recombination and hypermutation require activation-induced cytidine deaminase (AID), a potential RNA editing enzyme. Cell *102*, 553–563. https://doi.org/10.1016/s0092-8674(00)00078-7.
18. Diaz, M., Velez, J., Singh, M., Cerny, J., and Flajnik, M.F. (1999). Mutational pattern of the nurse shark antigen receptor gene (NAR) is similar to that of mammalian Ig genes and to spontaneous mutations in evolution: the translesion synthesis model of somatic hypermutation. Int. Immunol. *11*, 825–833. https://doi.org/10.1093/intimm/11.5.825.
19. Greenberg, A.S., Avila, D., Hughes, M., Hughes, A., McKinney, E.C., and Flajnik, M.F. (1995). A new antigen receptor gene family that undergoes rearrangement and extensive somatic diversification in sharks. Nature *374*, 168–173. https://doi.org/10.1038/374168a0.
20. Zou, J., Redmond, A.K., Qi, Z., Dooley, H., and Secombes, C.J. (2015). The CXC chemokine receptors of fish: insights into CXCR evolution in the vertebrates. Gen. Comp. Endocrinol. *215*, 117–131. https://doi.org/10.1016/j.ygcen.2015.01.004.
21. Rouvier, E., Luciani, M.F., and Golstein, P. (1993). Fas involvement in Ca(2+)-independent T cell-mediated cytotoxicity. J. Exp. Med. *177*, 195–200. https://doi.org/10.1084/jem.177.1.195.
22. Kägi, D., Vignaux, F., Ledermann, B., Bürki, K., Depraetere, V., Nagata, S., Hengartner, H., and Golstein, P. (1994). Fas and perforin pathways as major mechanisms of T cell-mediated cytotoxicity. Science *265*, 528–530. https://doi.org/10.1126/science.7518614.
23. Peperzak, V., Veraar, E.A.M., Xiao, Y., Babala, N., Thiadens, K., Brugmans, M., and Borst, J. (2013). CD8+ T cells produce the chemokine CXCL10 in response to CD27/CD70 costimulation to promote generation of the CD8+ effector T cell pool. J. Immunol. *191*, 3025–3036. https://doi.org/10.4049/jimmunol.1202222.
24. Melichar, H.J., Narayan, K., Der, S.D., Hiraoka, Y., Gardiol, N., Jeannet, G., Held, W., Chambers, C.A., and Kang, J. (2007). Regulation of gammadelta versus alphabeta T lymphocyte differentiation by the transcription factor SOX13. Science *315*, 230–233. https://doi.org/10.1126/science.1135344.
25. Hirano, M., Guo, P., McCurley, N., Schorpp, M., Das, S., Boehm, T., and Cooper, M.D. (2013). Evolutionary implications of a third lymphocyte lineage in lampreys. Nature *501*, 435–438. https://doi.org/10.1038/nature12467.
26. Venkatesh, B., Lee, A.P., Ravi, V., Maurya, A.K., Lian, M.M., Swann, J.B., Ohta, Y., Flajnik, M.F., Sutoh, Y., Kasahara, M., et al. (2014). Elephant shark genome provides unique insights into gnathostome evolution. Nature *505*, 174–179. https://doi.org/10.1038/nature12826.

27. Redmond, A.K., Macqueen, D.J., and Dooley, H. (2018). Phylotranscriptomics suggests the jawed vertebrate ancestor could generate diverse helper and regulatory T cell subsets. BMC Evol. Biol. *18*, 169. https://doi.org/10.1186/s12862-018-1290-2.

28. Pettinello, R., Redmond, A.K., Secombes, C.J., Macqueen, D.J., and Dooley, H. (2017). Evolutionary history of the T cell receptor complex as revealed by small-spotted catshark (Scyliorhinus canicula). Dev. Comp. Immunol. *74*, 125–135. https://doi.org/10.1016/j.dci.2017.04.015.

29. Kim, C.H., Rott, L.S., Clark-Lewis, I., Campbell, D.J., Wu, L., and Butcher, E.C. (2001). Subspecialization of CXCR5+ T cells: B helper activity is focused in a germinal center-localized subset of CXCR5+ T cells. J. Exp. Med. *193*, 1373–1381. https://doi.org/10.1084/jem.193.12.1373.

30. Nurieva, R.I., Chung, Y., Hwang, D., Yang, X.O., Kang, H.S., Ma, L., Wang, Y.h., Watowich, S.S., Jetten, A.M., Tian, Q., et al. (2008). Generation of T follicular helper cells is mediated by interleukin-21 but independent of T helper 1, 2, or 17 cell lineages. Immunity *29*, 138–149. https://doi.org/10.1016/j.immuni.2008.05.009.

31. Lee, A.Y.S., Reimer, D., Zehrer, A., Lu, M., Mielenz, D., and Körner, H. (2017). Expression of membrane-bound CC chemokine ligand 20 on follicular T helper cells in T-B-cell conjugates. Front. Immunol. *8*, 1871. https://doi.org/10.3389/fimmu.2017.01871.

32. Kageyama, R., Cannons, J.L., Zhao, F., Yusuf, I., Lao, C., Locci, M., Schwartzberg, P.L., and Crotty, S. (2012). The receptor Ly108 functions as a SAP adaptor-dependent on-off switch for T cell help to B cells and NKT cell development. Immunity *36*, 986–1002. https://doi.org/10.1016/j.immuni.2012.05.016.

33. Dijkstra, J.M. (2014). TH2 and Treg candidate genes in elephant shark. Nature *511*, E7–E9. https://doi.org/10.1038/nature13446.

34. Krautler, N.J., Kana, V., Kranich, J., Tian, Y., Perera, D., Lemm, D., Schwarz, P., Armulik, A., Browning, J.L., Tallquist, M., et al. (2012). Follicular dendritic cells emerge from ubiquitous perivascular precursors. Cell *150*, 194–206. https://doi.org/10.1016/j.cell.2012.05.032.

35. Heesters, B.A., Chatterjee, P., Kim, Y.-A., Gonzalez, S.F., Kuligowski, M.P., Kirchhausen, T., and Carroll, M.C. (2013). Endocytosis and recycling of immune complexes by follicular dendritic cells enhances B cell antigen binding and activation. Immunity *38*, 1164–1175. https://doi.org/10.1016/j.immuni.2013.02.023.

36. Suzuki, K., Grigorova, I., Phan, T.G., Kelly, L.M., and Cyster, J.G. (2009). Visualizing B cell capture of cognate antigen from follicular dendritic cells. J. Exp. Med. *206*, 1485–1493. https://doi.org/10.1084/jem.20090209.

37. Steiner, T.M., Heath, W.R., and Caminschi, I. (2022). The unexpected contribution of conventional type 1 dendritic cells in driving antibody responses. Eur. J. Immunol. *52*, 189–196. https://doi.org/10.1002/eji.202149658.

38. Cao, W., Lee, S.H., and Lu, J. (2005). CD83 is preformed inside monocytes, macrophages and dendritic cells, but it is only stably expressed on activated dendritic cells. Biochem. J. *385*, 85–93. https://doi.org/10.1042/BJ20040741.

39. Reyes, R., Cardeñes, B., Machado-Pineda, Y., and Cabañas, C. (2018). Tetraspanin CD9: a key regulator of cell adhesion in the immune system. Front. Immunol. *9*, 863. https://doi.org/10.3389/fimmu.2018.00863.

40. Peng, W.M., Yu, C.F., Kolanus, W., Mazzocca, A., Bieber, T., Kraft, S., and Novak, N. (2011). Tetraspanins CD9 and CD81 are molecular partners of trimeric FcεRI on human antigen-presenting cells. Allergy *66*, 605–611. https://doi.org/10.1111/j.1398-9995.2010.02524.x.

41. Kocks, C., and Rajewsky, K. (1988). Stepwise intraclonal maturation of antibody affinity through somatic hypermutation. Proc. Natl. Acad. Sci. USA *85*, 8206–8210. https://doi.org/10.1073/pnas.85.21.8206.

42. Matz, H., and Dooley, H. (2019). Shark IgNAR-derived binding domains as potential diagnostic and therapeutic agents. Dev. Comp. Immunol. *90*, 100–107. https://doi.org/10.1016/j.dci.2018.09.007.

43. Kabat, E.A., Wu, T.T., and Bilofsky, H. (1977). Unusual distributions of amino acids in complementarity-determining (hypervariable) segments of heavy and light chains of immunoglobulins and their possible roles in specificity of antibody-combining sites. J. Biol. Chem. *252*, 6609–6616.

44. Zapata, A.g., Torroba, M., Sacedón, R., Varas, A., and Vicente, A. (1996). Structure of the lymphoid organs of elasmobranchs. J. Exp. Zool. *275*, 125–143. https://doi.org/10.1002/(SICI)1097-010X(19960601/15)275:2/3<125::AID-JEZ6>3.0.CO;2-F.

45. Zapata, A., and Amemiya, C.T. (2000). Phylogeny of lower vertebrates and their immunological structures. In Origin and Evolution of the Vertebrate Immune System Current Topics in Microbiology and Immunology, L. Du Pasquier and G.W. Litman, eds. (Springer), pp. 67–107. https://doi.org/10.1007/978-3-642-59674-2_5.

46. Muthupandian, A., Waly, D., and Magor, B.G. (2021). Do ectothermic vertebrates have a home in which to affinity mature their antibody responses? Dev. Comp. Immunol. *119*, 104021. https://doi.org/10.1016/j.dci.2021.104021.

47. Lee, S.S., Tranchina, D., Ohta, Y., Flajnik, M.F., and Hsu, E. (2002). Hypermutation in shark immunoglobulin light chain genes results in contiguous substitutions. Immunity *16*, 571–582. https://doi.org/10.1016/s1074-7613(02)00300-x.

48. Liu, J., and Shulman, Z. (2022). Affinity-based clonal selection in Peyer's patches. Curr. Opin. Immunol. *74*, 100–105. https://doi.org/10.1016/j.coi.2021.11.002.

49. Nowosad, C.R., Mesin, L., Castro, T.B.R., Wichmann, C., Donaldson, G.P., Araki, T., Schiepers, A., Lockhart, A.A.K., Bilate, A.M., Mucida, D., and Victora, G.D. (2020). Tunable dynamics of B cell selection in gut germinal centres. Nature *588*, 321–326. https://doi.org/10.1038/s41586-020-2865-9.

50. Martinez-Riano, A., Wang, S., Boeing, S., Minoughan, S., Casal, A., Spillane, K.M., Ludewig, B., and Tolar, P. (2022). Long-term retention of antigens in germinal centres is controlled by the spatial organisation of the follicular dendritic cell network. Preprint at bioRxiv. https://doi.org/10.1101/2022.09.06.506650.

51. Garg, A.K., Mitra, T., Schips, M., Bandyopadhyay, A., and Meyer-Hermann, M. (2022). Amount of antigen, T follicular helper cells and quality of seeder cells shape the diversity of germinal center B cells. Preprint at bioRxiv. https://doi.org/10.1101/2022.10.26.513835.

52. Longo, N.S., and Lipsky, P.E. (2006). Why do B cells mutate their immunoglobulin receptors? Trends Immunol. *27*, 374–380. https://doi.org/10.1016/j.it.2006.06.007.

53. Yasuda, M., Taura, Y., Yokomizo, Y., and Ekino, S. (1998). A comparative study of germinal center: fowls and mammals. Comp. Immunol. Microbiol. Infect. Dis. *21*, 179–189. https://doi.org/10.1016/s0147-9571(98)00007-1.

54. Rumfelt, L.L., McKinney, E.C., Taylor, E., and Flajnik, M.F. (2002). The development of primary and secondary lymphoid tissues in the nurse shark Ginglymostoma cirratum: B-cell zones precede dendritic cell immigration and T-cell zone formation during ontogeny of the spleen. Scand. J. Immunol. *56*, 130–148. https://doi.org/10.1046/j.1365-3083.2002.01116.x.

55. Rueden, C.T., Schindelin, J., Hiner, M.C., DeZonia, B.E., Walter, A.E., Arena, E.T., and Eliceiri, K.W. (2017). ImageJ2: ImageJ for the next generation of scientific image data. BMC Bioinf. *18*, 529. https://doi.org/10.1186/s12859-017-1934-z.

56. Dobin, A., Davis, C.A., Schlesinger, F., Drenkow, J., Zaleski, C., Jha, S., Batut, P., Chaisson, M., and Gingeras, T.R. (2013). STAR: ultrafast universal RNA-seq aligner. Bioinformatics *29*, 15–21. https://doi.org/10.1093/bioinformatics/bts635.

57. McGinnis, C.S., Murrow, L.M., and Gartner, Z.J. (2019). DoubletFinder: doublet detection in single-cell RNA sequencing data using artificial nearest neighbors. Cell Syst. *8*, 329–337.e4. https://doi.org/10.1016/j.cels.2019.03.003.

58. Hao, Y., Hao, S., Andersen-Nissen, E., Mauck, W.M., Zheng, S., Butler, A., Lee, M.J., Wilk, A.J., Darby, C., Zager, M., et al. (2021). Integrated analysis

of multimodal single-cell data. Cell *184*, 3573–3587.e29. https://doi.org/10.1016/j.cell.2021.04.048.

59. Korsunsky, I., Millard, N., Fan, J., Slowikowski, K., Zhang, F., Wei, K., Baglaenko, Y., Brenner, M., Loh, P.-R., and Raychaudhuri, S. (2019). Fast, sensitive and accurate integration of single-cell data with Harmony. Nat. Methods *16*, 1289–1296. https://doi.org/10.1038/s41592-019-0619-0.
60. Bolotin, D.A., Poslavsky, S., Mitrophanov, I., Shugay, M., Mamedov, I.Z., Putintseva, E.V., and Chudakov, D.M. (2015). MiXCR: software for comprehensive adaptive immunity profiling. Nat. Methods *12*, 380–381. https://doi.org/10.1038/nmeth.3364.
61. Bakke, F.K., Gundappa, M.K., Matz, H., Stead, D.A., Macqueen, D.J., and Dooley, H. (2022). Exploration of the nurse shark (Ginglymostoma cirratum) plasma immunoproteome using high-resolution LC-MS/MS. Front. Immunol. *13*, 873390. https://doi.org/10.3389/fimmu.2022.873390.
62. Drokhlyansky, E., Smillie, C.S., Van Wittenberghe, N., Ericsson, M., Griffin, G.K., Eraslan, G., Dionne, D., Cuoco, M.S., Goder-Reiser, M.N., Sharova, T., et al. (2020). The human and mouse enteric nervous system at single-cell resolution. Cell *182*, 1606–1622.e23. https://doi.org/10.1016/j.cell.2020.08.003.
63. Slyper, M., Porter, C.B.M., Ashenberg, O., Waldman, J., Drokhlyansky, E., Wakiro, I., Smillie, C., Smith-Rosario, G., Wu, J., Dionne, D., et al. (2020). A single-cell and single-nucleus RNA-Seq toolbox for fresh and frozen human tumors. Nat. Med. *26*, 792–802. https://doi.org/10.1038/s41591-020-0844-1.

STAR★METHODS

KEY RESOURCES TABLE

REAGENT or RESOURCE	SOURCE	IDENTIFIER
Antibodies		
Monoclonal antibody supernatant GA10	Rumfelt et al.[54]	N/A
Monoclonal antibody supernatant NARV	Rumfelt et al.[54]	N/A
Monoclonal antibody supernatant LK14	Rumfelt et al.[54]	N/A
TotalSeq™-B0911 anti-phycoerythrin (PE) Antibody	BioLegend	Cat#408113; RRID:AB_2888824
Anti-Mouse IgG (H + L), CF™ 488A antibody produced in goat	Sigma-Aldrich	SKU SAB4600042; RRID:AB_2532075
Chemicals, peptides, and recombinant proteins		
R-phycoerythrin	Invitrogen	Cat#P801
Freund's Adjuvant, Complete	Sigma-Aldrich	SKU F5881
Tricaine methanesulfonate	Syndel	Syncaine®
SuperScript™ II Reverse Transcriptase	Invitrogen	Cat#18064022
Critical commercial assays		
RNAscope Multiplex Fluorescent V2 Assay	Advanced Cell Diagnostics	Cat#323100
Chromium Next GEM Single Cell 3′ GEM, Library & Gel Bead Kit v3.1	10X Genomics	PN-1000121
Chromium Single Cell A Chip Kit	10X Genomics	N/A
Arcturus PicoPure RNA Isolation Kit	Applied Biosystems	Cat#KIT0204
Qubit RNA Broad-Range Assay Kit	Invitrogen	Cat#Q10210
Deposited data		
Nurse shark *Aicda*	This paper	NCBI: OM746124
Whale shark (*Rhincodon typus*) reference genome	Emory University	NCBI: ASM164234v2
Nurse shark VNAR sequence reads	This paper	NCBI: PRJNA963203
Nurse shark spleen snRNA seq dataset	This paper	NCBI: GSE232302
Experimental models: Organisms/strains		
Nurse sharks (*Ginglymostoma cirratum*)	Wild caught	N/A
Oligonucleotides		
RNAscope® Probe- Gc-AR	Advanced Cell Diagnostics	Cat#811971
RNAscope® Probe- Gc-CD3e-C2	Advanced Cell Diagnostics	Cat#821911-C2
RNAscope® Probe- Gc-CXCR4-C3	Advanced Cell Diagnostics	Cat#829241-C3
RNAscope® Probe- Gc-CXCR5	Advanced Cell Diagnostics	Cat#849161
RNAscope® Probe- Gc-AID-C2	Advanced Cell Diagnostics	Cat#821921-C2
RNAscope® Probe- Gc-MKI67-C3	Advanced Cell Diagnostics	Cat#1198291-C3
NAR-Fr1-forward AGACGGGCGAATCACTGACC	This paper	N/A
NAR-Fr5-reverse TATTCCAGGATTCACAGTCACGAC	This paper	N/A
Software and algorithms		
Affinity Photo	Serif	https://affinity.serif.com/en-us/photo/
ImageJ2	Rueden et al.[55]	https://imagej.net/software/fiji/downloads
StarSolo v2.7.7a	Dobin et al.[56]	https://github.com/alexdobin/STAR/blob/master/docs/STARsolo.md
DoubletFinder v2.0	McGinnis et al.[57]	https://github.com/chris-mcginnis-ucsf/DoubletFinder

(*Continued on next page*)

Continued

REAGENT or RESOURCE	SOURCE	IDENTIFIER
Seurat v4.0.4	Hao et al.[58]	https://satijalab.org/seurat/
Harmony v0.1.0	Korsunsky et al.[59]	https://github.com/immunogenomics/harmony/blob/master/NEWS
MiXCR	Bolotin et al.[60]	https://github.com/milaboratory/mixcr
Other		
Opal 520 Reagent Pack	Akoya Biosciences	SKU FP1487001KT
Opal 620 Reagent Pack	Akoya Biosciences	SKU FP1495001KT

RESOURCE AVAILABILITY

Lead contact

Further information and requests for resources and reagents should be directed to the lead contact, Dr. Helen Dooley (hdooley@som.umaryland.edu).

Materials availability

This study did not generate new unique reagents.

Data and code availability

- The VNAR reads generated during the current study have been deposited with NCBI: PRJNA963203. The snRNA seq data have been deposited in the NCBI GEO database: GSE232302. All other data generated or analyzed during this study are included in this published article or its supplementary information files.
- This paper does not report original code.
- Any additional information required to reanalyze the data reported in this work paper is available from the lead contact upon request.

EXPERIMENTAL MODEL AND STUDY PARTICIPANT DETAILS

Animals

Nurse sharks (*Ginglymostoma cirratum*), male and female, aged between 2 and 3 years and averaging 1.2 kg in weight, were acquired from Florida coastal waters under a Special Activity License granted by the Florida Fish and Wildlife Conservation Commission. Animals were acclimatized in 12,000L indoor tanks containing continuously recirculating artificial sea water at 28°C, at the Institute of Marine and Environmental Technology (IMET), Baltimore, USA, for at least 3 months prior to immunization and sampling. All experimental procedures were conducted in accordance with University of Maryland, School of Medicine Institutional Animal Care and Use Committee (IACUC) approved protocols. A mix of male and female nurse sharks were used for this study however sex differences have not been reported for any study of shark adaptive immunity performed to date.

METHOD DETAILS

Shark immunizations and sample collection

Sharks were immunized subcutaneously in the ventral side of the pectoral fin with 300 μg R-phycoerythrin (PE) emulsified in Freund's complete adjuvant. Individual animals were sacrificed by an overdose of tricaine methanesulfonate (MS-222) at day (D)10, D30, D40, or D50 post-immunization. Tissue samples for microscopy experiments were collected and frozen in Tissue-Tek optimum cutting temperature (OCT) compound (Sakura). Tissue samples for single nucleus RNA sequencing were collected and flash frozen in liquid nitrogen. Samples were stored at −80°C prior to use.

Immunofluorescence microscopy

Frozen tissue samples were sectioned on a Tissue-Tek Cryo3 cryostat (Sakura) at 6 μm thickness, mounted on Superfrost Plus microscope slides (VWR), and fixed for 30 s in 100% acetone. During immunofluorescence staining, care was taken to keep slides in the dark to prevent photobleaching of PE. Slides were rehydrated in PBS for 5 min, then permeabilized in 0.05% Tween 20 PBS (PBST) for 45 min at 4°C. Slides were blocked for 45 min in 10% fetal bovine serum (FBS)/PBST at 4°C, then washed in PBST for 5 min. Slides were then incubated with anti-nurse shark IgNAR (GA10 or NARV) or anti-nurse shark IgL (LK14) monoclonal antibody supernatant[54] or anti-PE antibody (BioLegend) diluted 1:250 in 2% FBS/PBST for 1 h at 4°C. Slides incubated with isotype-matched antibody or

Dulbecco's Modified Eagle Medium (DMEM) supernatant were included as negative controls. Following incubation, the slides were washed with PBST, then incubated with secondary goat anti-mouse IgG-Alexa Fluor 488 (Sigma Aldrich) 1:250 in 2% FBS/PBST for 1 h at 4°C. Slides were washed in PBST, then mounted in ProLong Gold + DAPI (ThermoFisher). Microscopy was performed on an Echo Revolve fluorescence microscope equipped with necessary filters. Images were edited for brightness and contrast and composite images produced using Affinity Photo software. Scale bars were added using Fiji (ImageJ2) software.[55] Tissue areas were measured using the Echo Revolve software.

Fluorescence *in situ* hybridization (FISH)

Fluorescence in situ hybridization (FISH) experiments were performed using Advanced Cell Diagnostics RNAscope Multiplex Fluorescent V2 Assay. RNA FISH probes were designed and manufactured by Advanced Cell Diagnostics for nurse shark sequences *Ignar*,[19] *Cd3e*,[28] *Cxcr4* and *Cxcr5*,[20] *Aicda* (GenBank: OM746124), and *Mki67* from a nurse shark transcriptome produced by our lab.[61] Assays were performed according to the manufacturer's instructions. In brief, fresh frozen tissue samples were sectioned at 6 μm thickness, mounted on microscope slides, then fixed in 10% neutral buffered formalin at 4°C. Tissue slides were dehydrated in 50%, 75%, and 100% ethanol, treated with hydrogen peroxidase and RNAscope Protease IV, then hybridized with target gene probes for 2 h at 40°C. Negative control probes provided by the manufacturer and targeting bacterial DapB gene in all multiplex channels were included. Tissue slides were then hybridized with amplification probes and multiplex channels developed individually using assay reagents. Opal 520 and 620 fluorophores (Akoya Biosciences) were used at 1:1000 dilutions determined by previous experiments based on target gene signal intensity. Tissue slides were stained with DAPI then mounted in ProLong Gold + DAPI or ProLong Glass + NucBlue. Microscopy was performed on an Echo Revolve fluorescence microscope equipped with necessary filters. Images were edited for brightness and contrast using Affinity Photo software. Scale bars were added using Fiji (ImageJ2) software.

snRNA-seq data generation and analysis

A protocol adapted from[62] was used for nuclear extraction, employing a Tween with salts and tris (TST) buffer, which has been shown to perform well in recovering high cell type diversity across sample types.[63] Approximately 45 mg of each frozen spleen sample was placed in a 6-well tissue culture plate (Stem Cell Technologies) with 1 mL TST (2 mL of 2X ST buffer +120 μL of 1% Tween 20 + 20 μL of 2% BSA brought up to 4 mL with nuclease-free water). The tissue was minced using Noyes Spring Scissors for 10 min on ice. The resulting homogenate was filtered through a 40 μm Falcon cell strainer, and a further 1 mL of TST was added to wash the well and filter. The volume was brought up to 5 mL using 3 mL of 1X ST buffer (diluted from 2xST buffer [292 μL of 146 mM NaCl, 100 μL of 10 mM Tris-HCl pH 7.5, 10 μL of 1 mM CaCl2, 210 μL of 21 mM MgCl2, brought up to 10 mL with nuclease-free water]). The sample was centrifuged at 4°C for 5 min at 500 g before the resulting pellet was re-suspended in 1 mL 1X ST buffer and the recovered nuclei were filtered through a 40 μm Falcon cell strainer.

The nuclei were processed through the ChromiumTM Single Cell Platform using the ChromiumTM Single Cell 30 Library and Gel Bead Kit v3.1 and ChromiumTM Single Cell A Chip Kit (both 10X Genomics) as per the manufacturer's protocol. Briefly, the isolated nuclei were stained with Hoechst die and their integrity visually confirmed under a fluorescent microscope. The nuclei were counted using a Bio-Rad TC20, and approximately 7,000 loaded per sample into a channel of a Chromium 3′ Chip. The nuclei were partitioned into droplets using the Chromium controller before the captured RNA for each nucleus was barcoded and reverse transcribed. The resulting cDNA was PCR amplified for 14 cycles, fragmented, and size selected before Illumina sequencing adaptor and sample indexes were attached. Libraries were sequenced on a NovaSeq 6000 platform by Novogene UK Ltd, resulting in ~220 million paired end 2x150bp reads per sample.

As the closest related shark species with a published reference genome, the genome of the whale shark (*Rhincodon typus*; NCBI: ASM164234v2) was used for alignment and feature counting. Sequences for five nurse shark genes of specific interest but absent from the whale shark genome annotation, were appended to the genome annotation GTF file (*Aicda*, *Cd79a*, *Il21*, and two *Tnfsf13b* paralogs). StarSolo v2.7.7a[56] was used to align reads with the following changes to default settings: –soloUMIdedup 1MM_Directional, –soloCellFilter TopCells 25000, –outFilterMatchNminOverLread 0.15, –outFilterScoreMinOverLread 0.15, –outMultimapperOrder Random, –soloFeatures GeneFull. Reads mapping to introns were retained to account for the large quantity of unspliced transcripts present in snRNA-seq data and the top 25,000 nuclei by UMI count were retained to ensure retention of the transcriptionally quiet erythrocytes. To account for sequence dissimilarity between whale shark and nurse shark, the alignment filtering thresholds –outFilterMatchNminOverLread and –outFilterScoreMinOverLread, corresponding to minimum alignment length and alignment score were optimized to return the highest UMI per nuclei and genes per nucleus. A score of 0.15 was found to be optimal for these parameters (Table S2).

Quality control was performed on each sample separately. Genes expressed in fewer than five nuclei were excluded. Nuclei with fewer than 500 genes or 800 UMIs were excluded. Gene expression was normalized by dividing the UMI count for each gene by the total UMI for each nucleus, multiplying by 1000 and applying the function ln(1 + x). DoubletFinder v2.0[57] was used to identify and remove potential doublets using preliminary clustering to simulate doublet expression.

Clustering and visualization were performed using Seurat v4.0.4.[58] The expression matrices of both samples were concatenated, and dimensionality reduction performed using principal component analysis (PCA) restricted to the 2,000 most variable genes. Batch correction between samples was performed with Harmony v0.1.0,[59] and the first 35 PCA components in the batch corrected space were used to cluster nuclei using the shared nearest neighbor approach in Seurat. UMAP visualizations were generated using the

'RunUMAP' command in Seurat. Broad cellular identity was established by performing a differential gene expression test for each population against all other populations and checking against a panel of known marker genes for each lineage (Table S4). A separate analysis of T cells was conducted by sub-setting the nuclei identified as T cells in the global analysis, recalculating the 2,000 most variable genes within the T cells, and repeating the same dimensionality reduction, PCA, batch correction and clustering steps (using 11 PCA components). A population of potential T cell/B cell doublets were manually removed at this stage, based on an expression profile consistent with both T cells and B cells and a lack of marker genes unique to that population. All differential gene expression tests used a Wilcoxon Rank-Sum test with a minimum log2-fold change threshold of 0.25 and expression in at least 20% of cells in a cluster.

Rapid immunofluorescence staining and laser microdissection (LMD)

A rapid immunofluorescence staining protocol was developed to quickly identify IgNAR+ B cells while preserving sample RNA integrity. Frozen spleen samples were sectioned on a Tissue-Tek Cryo3 cryostat (Sakura) at 6 μm thickness and adhered to polyethylene naphthalate (PEN) metal frame slides (Leica), 2 sections per microscope slide. Under RNase free conditions, sections were fixed in ice-cold acetone for 30 s. After briefly air drying, sections were stained for 90 s with cell culture supernatant containing anti-nurse shark IgNAR monoclonal supernatant and supplemented with RNasin Ribonuclease Inhibitor (1 U/μl, Promega). Slides were rinsed in RNAse-free PBS, then incubated with goat anti-mouse Alexa Fluor 488 diluted 1:100 in 2% FBS/PBS supplemented with RNasin (1 U/μl) for 90 s. Slides were rinsed in RNAse-free PBS and then air dried for 7 min. The slides were visualized and 10–15 IgNAR$^+$ B cell follicles extracted using a Leica LMD7 microscope equipped with the necessary filters. Sections were collected into the caps of 0.2 mL microcentrifuge tubes containing 25 μL Arcturus PicoPure Extraction Buffer. Once LMD isolation was complete, the tubes were capped and centrifuged, collecting the samples into a further 25 μL of extraction buffer. Tubes were immediately snap frozen on dry ice until ready for RNA purification. Upon thawing the sample, RNA was purified using the Arcturus PicoPure RNA Isolation Kit (Thermo Scientific) according to the manufacturer's protocol for fresh frozen tissues. RNA concentration was assessed using a Qubit 3 fluorometer and Qubit RNA Broad-Range Assay Kit (Invitrogen).

LMD IgNAR variable region repertoire data generation and analysis

SuperScript II Reverse Transcriptase (RT) was used to generate cDNA from the extracted RNA following the manufacturer's instructions (Invitrogen). The total RNA sample (12 μL containing 62 ng of RNA) was combined with 1 μL of 0.5 μg/μL Oligo(dT)12–18 primer and 1 μL of 10 mM dNTP mix, incubated for 5 min at 65°C, then placed on ice. Next, 4 μL 5X First-Strand Buffer and 2 μL 0.1 M DTT were added to the reaction, mixed, and incubated for 2 min at 42°C. Finally, 1 μL SuperScript RT and 1 μL DEPC H2O were added to the reaction, mixed, and incubated at 42°C for 1 h and the reaction inactivated by heating to 70°C for 15 min.

The cDNA produced above was used as input for PCR reactions to generate a library of IgNAR variable regions (VNARs) present in the LMD-extracted follicles. A set of 3 reactions were prepared, each containing 20 ng of cDNA, and VNAR sequences were amplified by PCR using the framework-annealing primers NAR-Fr1-forward (5′-AGACGGGCGAATCACTGACC-3′) and NAR-Fr5-reverse (5′-TATTCCAGGATTCACAGTCACGAC-3′) which give a product of 270–290 bp. PCR cycling conditions were as follows: 1 cycle at 95°C for 1 min, 30 cycles at 95°C for 30 s, 55°C for 30 s, 72°C for 1 min, and 1 cycle at 72°C for 2 min. After amplifying the VNAR sequences, the reactions were pooled, and the PCR products cleaned up following the QIAquick PCR Purification Kit protocol (Qiagen). The VNAR library was sequenced on an Illumina NovaSeq 6000 platform by Novogene USA Ltd., resulting in ~22.5 million paired-end 2x150bp reads.

Standard Ig repertoire analyses typically involves aligning sequencing reads to reference datasets of germline V(D)J alleles. Shark Ig repertoires have never been assessed using high-throughput sequencing methods, so it was necessary to prepare suitable reference data for analyses with existing tools. Notably, the V gene region of IgNAR is reported to incorporate seven distinct subsegments: a single complementarity determining region (CDR1) and two hypervariable segments (HV2 and HV4), surrounded by framework regions (FR1-4). Thus, unlike the human V region formation of FR1-CDR1-FR2-CDR2-FR3, shark IgNAR takes the form FR1-CDR1-FR2-HV2-FR3-HV4-FR4 [43]. This lack of direct correspondence with human subregions complicates reference formatting.

We used MiXCR (version 3.0.3)[60] to align and extract the IgNAR V regions, in part because it can accept data from new reference species, which relies on the reseqio JSON format (https://github.com/repseqio/repseqio/wiki/repseqio-JSON-library-format) for reference species. To enable reference formatting, we encoded the HV2-FR3-HV4 subsection of the IgNAR V gene as CDR2, as they together occupy the equivalent position to CDR2 in humans, with the intention of separating these sections after MiXCR alignment. This had the effect that FR4 at the end of the shark IgNAR V was encoded as FR3 (occupying the equivalent position), and IgNAR FR5 (which follows the J segment) was encoded as its positional equivalent in humans, FR4. We encoded the three nurse shark IgNAR Vs. (type I, II, and III) using this approach.

The MiXCR 'align' function was then used on the LMD VNAR library reads, specifying nurse shark for both the reference library and species. Following this, we used the 'exportAlignments' function in MiXCR to extract sequence and mutation information for the 7 distinct regions of the IgNAR V genes from the resultant alignment data. Considering the reference file subsegment definitions work-around described above, we could not extract all seven IgNAR V subregions using their correct names, but rather used the above prescribed positional equivalents in humans. Direct human-like naming convention was possible for FR1, CDR1, and FR2, for which we extracted amino acid sequences using the –aaFeature command (e.g., '-aaFeature CDR1' would recover the CDR1 sequence segment for each alignment). As the shark IgNAR HV2-FR3-HV4 region was encoded as though it were human CDR2,

extracting these segments required further manipulation by specifying subsection of the encoded CDR2. For this we used the following commands: '-aaFeature {CDR2:Begin:CDR2Begin(+30)}' to recover the sequence from the start of CDR2 up to 30 nucleotides into the CDR2 which corresponds to the 10 amino acid HV2 region, '-aaFeature {CDR2Begin(+30):CDR2Begin(+51)}' to recover next the 7 amino acids which form the IgNAR FR3 region, and '-aaFeature {CDR3Begin(+51):FR3Begin}' (For this flag recall that IgNAR FR4 is encoded as FR3, its human equivalent) to recover the remainder of the CDR2 encoded region as HV4). The FR4 region of IgNAR, which was offset to appear as FR3 by the HV2-FR3-HV4 recoding to CDR2 was then recovered using '-aaFeature FR3'. Mutation data corresponding to replacement and silent mutations was extracted using the same approach, but this time preceding the region of interest with the '-mutationsDetailed' flag rather than '-aaFeature'.

To ensure that our analyses focused on fully intact sequences we exported full length sequences on the amino acid and nucleotide levels using the flags '-aaFeature {FR1Begin:FR4End}' and '-aaFeature {FR1Begin:FR4End}' (where FR4 refers to the shark IgNAR FR5 which comes after the rearranged CDR3 region), and then used bash commands to filter out partial sequences and sequences interrupted by frameshifts or premature stop codons. Importantly, as we wished to assess V segment amino acid variability and R/S ratios (i.e., selection) we did not cluster sequences into clonotype groups of closely related sequences. Instead, to fully assess replacement and silent mutations in the data we considered two sequences separated by even a single nucleotide change (including those that do not result in amino acid changes) across the full length of the sequence (i.e., start of FR1 to end of the post-CDR3 FR5) as distinct sequences. As a result of this we incorporated an extra control step (to reduce the possibility of mistaking sequencing errors from true mutations); we retained only those nucleotide alignments that were recovered at least 10 times as a V sequence for further analysis. Bash commands were then used to select for aligned sequences that did not deviate in length across any of the seven subregions to help avoid errors in downstream analyses (and to promote equal treatment between these subregions as our region encoding and extraction approach already does this to a certain degree for the HV2, FR3, and HV4 regions), to extract V sequence counts, and the top 100 most abundant distinct V sequences, as well as to export summary data for amino acid variability analyses, and replacement and silent mutation data for calculations and graphical presentation in Microsoft Excel and R (v3.3.2). Amino acid variability was calculated using the Wu-Kabat Variability Coefficient[43] in Excel with the amino acid sequence data extracted from the MiXCR 'exportAlignments' output, while a one-sided Wilcoxon rank-sum test was performed with the wilcox.test function in R to assess whether variability is greater in CDR/HV regions as compared to FR regions in the V gene. R/S ratios for CDR/HV and FR were assessed by dividing the inferred replacement mutations by the inferred silent mutations extracted from the MiXCR 'exportAlignments' output. An additional subset of mutations was also identified, but not included in the main analyses, for which the order of mutation events is important to determining whether the mutation is a replacement or silent mutation. We performed extra R/S ratio analyses encoding all of these ambiguous mutations as either replacement or silent (representing the two extreme possibilities for the data) and found that this did not change the overall outcome of our results. For all R/S analyses each unique mutation was treated as occurring only once as we could not readily determine whether a given mutation arose multiple times independently.

QUANTIFICATION AND STATISTICAL ANALYSIS

Information on our statistical analyses and the software used to perform each are detailed in the relevant STAR Methods section. For the VNAR repertoire analysis displayed in Figures 4C and S3D a p value < 0.05 was considered statistically significant.